LAWRENCE
LIVERMORE
NATIONAL
LABORATORY

LLNL-TR-661774

Stimulated RAMAN Scattering Inside KDP Crystal Segments

W. Lee Smith, F. P. Milanovich

September 30, 2014

Disclaimer

This work performed under the auspices of the U.S. Department of Energy by Lawrence Livermore National Laboratory under Contract DE-AC52-07NA27344.

M. Henderson

470
28209

August 25, 1982
UVM 82-19/5629r

TO: Distribution

FROM: W. Lee Smith and F. P. Milanovich

SUBJECT: STIMULATED RAMAN SCATTERING INSIDE KDP CRYSTAL SEGMENTS

A literature search revealed no quantitative Raman information on KDP, so we began a collaboration to answer this question as a protective measure for Nova/Novette performence. Several sessions later, we have as good an answer for the stimulated Raman gain as we can get with this approach, and we describe that result and its repercussions for crystal arrays here.

In Section I of this report, we give the results. In Section II we examine the repercussions for KDP crystal array performance and examine a potential fix. In Section III, we outline a plan to measure the necessary parameters and find out if we really have a problem.

The authors are jointly responsible for section I; WLS is responsible for Sections II and III.

W. Lee Smith

W. Lee Smith

F. P. Milanovich

F. P. Milanovich

WLS/tj

August 25, 1982

Section I. Measurement of KDP Raman Spectrum and Calculation of Stimulated Raman Gain

The crystal used for this work was a Type II, 5 cm by 5 cm, early array crystal. Figure 1 shows the scattering geometry of this investigation. The Ar pump laser (488 nm, 20491 cm^{-1}) is linearly polarized. The arrow on the side of the crystal is the direction of the optic axis. The crystal is rotated by 90 degrees about the argon axis to go from orientation "e" to orientation "o", which are so denoted because the Argon beam propagates in the crystal as an extraordinary or ordinary wave, respectively. With these two orientations we get Raman information for all the waves involved in doubling and tripling. While we use the notation "o" and "e" for simplicity, it should be noted that our results do not apply to the ordinary and extraordinary rays for any orientation of KDP crystal, but only to Type-II cut ($\theta = 59^{o}$) KDP.

The measured spontaneous Raman spectrum for KDP is shown in Fig. 2. The display is Raman scattering strength (counts/sec) versus Raman frequency shift (wavenumbers). The two spectra overlaid in Fig. 2 are for polarized and depolarized scattering. The strong, narrow peak in the polarized spectrum at 915 cm^{-1} is the threat; the other peaks are not of interest.

A high-resolution scan of the 915 cm^{-1} peak is shown in Fig. 3a for the KDP "o" orientation, and in Fig. 3b for the "e" orientation. The FWHM spectral width is 20 cm^{-1} in both orientations. However, the scattering signal is 2.0 x stronger in the "o" orientation than in the "e" orientation. The instrumental bandwidth for these scans is less than 2 cm^{-1}.

You will surely recall that the stimulated Raman gain coefficient g (cm/W) at the center frequency of the Raman vibration is given by

$$g = \frac{16\pi^2 c^2 N}{\hbar n_s^2 \omega_s^3 \Gamma} \frac{\partial \sigma}{\partial \Omega} \quad , \qquad (1)$$

in terms of the differential Raman scattering cross section $\partial\sigma/\partial\Omega$ (cm^2), and is given by

$$g = \frac{8\pi^2 N \omega_s}{n_L n_s c^2 m \omega_R \Gamma} \left(\frac{\partial \alpha}{\partial q}\right)^2 \quad , \tag{2}$$

in terms of the normal-mode derivative of the polarizability $\partial\alpha/\partial q$ (cm^2). The notation is

N	= number density of scatterers (cm^{-3})
c	= vacuum light speed (cm/sec)
$\hbar$	= reduced Planck constant (J-sec)
n_s	= refractive index at the Stokes frequency
n_L	= refractive index at the laser frequency
ω_s	= Stokes angular frequency ($=\omega_L - \omega_R$)
ω_R	= Raman vibration angular frequency
Γ	= FWHM linewidth of Raman vibration (rad/sec, not cm^{-1})
m	= reduced mass of vibration (g)

and, for completeness,

$$\frac{\partial\sigma}{\partial\Omega} = \frac{\hbar \omega_s^4 n_s}{2m \omega_R c^4 n_L} \left(\frac{\partial \alpha}{\partial q}\right)^2 \tag{3}$$

It is appropriate to mention here that comparing numerical results from literature papers on stimulated scattering is treacherous. One must know the author's complete definition set, and it is rarely given. In particular, HWHM linewidth values are frequently used without notification, giving a 2x error opportunity. We have been unable to reproduce by calculation several entries in large, collected data tables in review articles[1,2] and we suspect that bandwidth-integrated Raman strengths have been mixed with peak strengths in such tables. Beware.

One further comment is appropriate here, regarding the overall frequency dependence of the SRS gain coefficient. Neglecting electronic resonances, $\partial\alpha/\partial q$ is frequency-independent. Hence the overall frequency dependence of the SRS gain coefficient is given in Eq. (2) -- g is proportional to ω_s. That is straightforward and to be used for comparing one stimulated Raman situation to another -- for comparing ω-, 2ω-, and 3ω-driven SRS in KDP, for example. However, when one uses measured spontaneous Raman information ($\partial\sigma/\partial\Omega$) to calculate gain coefficients, ω_s^4 enters, giving ω_s^{-3} overall dependence (Eq. 1). In this report, we have scaled numbers by ω_s, ω_s^4, and the combination ω_s^{-3}, and these remarks should help you follow. Now back to the main theme.

Equations 1 and 2 contain the linewidth Γ and the assumption of a Lorentzian lineshape for the Raman transition. So, to use Eqs. 1 and 2, one customarily integrates the Raman signal in frequency across the lineshape, substracts background, and then divides by Γ. In the work reported here, we found it preferable to narrow the spectral resolution of the spectrometer and record counts per wavenumber, versus wavenumber. This procedure allowed us to eliminate the lineshape assumption, and to compare different materials according to the parameter most basic to the stimulated process which is the peak counts per wavenumber, denoted S. So our S is analogous to the customary $\partial\sigma/\partial\Omega$ divided by Γ.

Since the work we report here involved the use of a reference material, it is appropriate to discuss how confident we are in the measurements made by others. Our primary reference material was benzene. Because of the difficulty of spectrally resolving the narrow line (width 2.3 cm^{-1}) of the 992 cm^{-1} mode of benzene, we used a secondary reference material, nitrobenzene (Fig. 4, width 6.6 cm^{-1}), as a backup. Crystal quartz (Fig. 5) was run as a second backup, but our confidence in the literature information on this material has since waned.

In Table 1, we list the several values of the SRS gain coefficient for benzene that have been published. The agreement looks good, and eight measurements are statistically large. However, only the first two

listings in Table 1 involved any sort of stimulated conditions. The last six were calculations based on spontaneous Raman data only. (Among these, the work of Skinner and Nilson[9] is the benchmark). So, any confidence in the absolute numbers for the gain coefficient must come from the work of Aussenegg et al.[3] and Colles[4] and from the general state of agreement between stimulated Raman theory and measurement in all materials -- in particular, gases[10] -- in well-controlled experiments. All in all, we feel that a reasonable estimate of the absolute accuracy of the gain coefficient (5.5 cm/GW for 532-nm pump) for the benzene 992-cm^{-1} mode is $\pm$ 35%.

Our spontaneous-Raman results are collected in Table 2. Data for Cargille 5610 and Halocarbon 56 index-matching fluids are included in Table 2 for connection with our earlier SRS work. SRS gain relative to that of benzene is listed in column G and is the product of the column D and F entries. The ratio of the peak cross sections per wavenumber for benzene and nitrobenzene is in reasonable agreement (15%) with Skinner and Nilson,[9] and we believe this is the single most reliable check we can have.

The KDP "e" and "o" entries in Table 2 are the major result of this study. We measured KDP on four separate runs to test our reproducibility, and are sure of our peak strength ratio values to $\pm$ 15%. Coupled with the uncertainty in the data set on the benzene absolute gain coefficient (Table 1), we believe the numbers of 0.21 cm/GW, for "e" KDP, and 0.42 cm/GW, for "o" KDP, are accurate to within $\pm$ 50%. All the entries in Table 2, except column J, are for 488-nm pump light. For general utility, we list in column J the absolute gain in these materials for 532-nm pump light.

The lowest entry in column J of Table 2 is Halocarbon 56. In fact, this fluid has the lowest SRS gain ever reported in any fluid, to the best of our knowledge, and that is the reason it was an excellent find for index-matching fluid for our arrays.

Compared to HC56, KDP has "e" and "o" gain about 2.3 and 4.6 times higher, respectively. KDP gain is low among other Raman-investigated

materials which are used for harmonic generation -- lithium niobate, lithium tantalate, barium sodium niobate -- and comparable or low compared to crystal quartz and calcite. Raman gain in other more recent harmonic generation materials such as urea, MAP, etc., have not been reported. We intend to track this subject. (Those interested in crystalline laser hosts will need to include Raman activity as a parameter in their considerations, as well.)

Section II. Repercussions of SRS in KDP for Nova/Novette 2ω and 3ω Performance

In Table 3 we list the KDP gain coefficient, converted with Eq. 2 to the relevant harmonic pump wavelengths of Nova/Novette. (For comparison we list in Table 4 the same quantities for Halocarbon 56 fluid). We can now evaluate the repercussions of these measurements for Nova/Novette.

The "official" Nova/Novette maximum output intensity at three wavelengths for several pulse durations are listed in Table 5 and graphed in Fig. 6. These numbers result from crystal thicknesses of 1 cm as elected at the recent Nova design review. These are mean, not peak intensities, i.e., ripple factor = unity. These intensities would be present inside the KDP crystal segments and would pump the stimulated Raman process.

Raman side-scattered light travels 20 cm per nanosecond in KDP -- the transit times for the 27-cm and 15-cm segments are 1.35 ns and 0.75 ns, respectively. Because of additional aspects of this problem for pulse durations long enough to allow more than one traversal across a crystal, we have divided the next discussion into single-traversal and multiple-traversal sections. In this report, all pulses are assumed square in time. i.e. no variation in I_m during pulse

SHORT-PULSE REGIME: SINGLE TRAVERSAL

Parameters for the short-pulse discussion are listed in Table 6. Since the SRS gain depends on pump wavelength and KDP orientation, Table 6 is organized according to eight different waves (A through H) involved in Type I and II doubling and Type II tripling. Although Type I doubling

is not planned for Nova/Novette for other reasons, parameters for that configuration are included for completeness. The intensity values listed in column 3, 4, and 5 are derived from the official numbers in Table 5 and Fig. 6. We list the SRS gain coefficient for each wave in column 6. In columns 7, 8 and 9, we list the product of gain coefficient times pump intensity times the effective length (L_{eff}) in the KDP, for three pulse durations. The quantity $gI_m L_{eff}$ drives the exponential growth of the side-scattered intensity at the Stokes frequency according to

$$I_{SRS} = I_{s0}\, e^{gI_m L_{eff}} \qquad (4)$$

where I_{s0} is the 'noise' intensity level at the Stokes frequency, contributed by spontaneous Raman scattering. The largest entry in columns 7-9 is for the 2ω drive for Type II tripling at 1.35 ns. Exp (22.1) is roughly 4×10^9.

Estimation of the spontaneous noise intensity I_{s0} relevant to the solid geometry of the crystal array is useful to further our discussion. I have made such estimates, and these were corroborated by J. Falk.* Large uncertainties are unavoidable in this estimation, arising principally from the difficulty of knowing the effective solid angle and mode count, and how these might be scrambled on reflection from edge surfaces. But we are able to continue by examining a range probable of I_{s0} of 0.001 to 0.100 W/cm^2, as listed in Table 7. We see there that 20 to 25 is the range of $gI_m L_{eff}$ sufficient to side-scatter ~ 0.1 GW/cm^2, several percent of the intensity present in the crystal.

Now, referring to columns 7 and 8 of Table 6, we can predict that in a 27-cm segment, waves G and H involved in tripling could cause trouble;

---

*The authors are grateful to J. Falk for several helpful discussions on Raman scattering.

with the ± 50% uncertainty in g, it is possible that wave E will cause trouble in doubling, as well. In the 15-cm KDP segment (column 9 in Table 6), waves G and H may cause trouble. We will calculate how much trouble after introducing the long-pulse features.

LONG-PULSE REGIME: MULTIPLE TRAVERSALS

Durations beyond 1.35 ns and 0.75 ns enable SRS originating at one edge of a crystal segment to propagate 27 cm or 15 cm, respectively, to the opposing edge, reflect, and experience further gain in additional passes across the KDP. We can extend Eq. (4) to account for multiple traversals:

$$I_{SRS} = \underbrace{(I_{s0}\, e^{gI_m L_1})}_{1^{st}\text{ traversal}} \underbrace{(R_{eff})\, e^{gI_m L_2}}_{2^{nd}} \underbrace{(R_{eff})\, e^{gI_m L_3}}_{3^{rd}} \quad \ldots \qquad (5)$$

where

$$\sum_i L_i = c\tau/n \qquad (6)$$

and where the last length in Eq. 5 may be a fraction of 27 or 15 cm. The refractive index n may be taken as 1.5 for purposes of this entire report.

From Eq. (5) we see the familiar point that a way to keep the long-pulse SRS situation from being more deleterious than the single-traversal situation is to have

$$R_{eff} \leq e^{-gI_m L} \; . \qquad (7)$$

Then the SRS gain would not grow beyond the single-traversal levels listed in Table 6, columns 8 and 9. The analogy with the amplified spontaneous emission problem in disks is very strong.

Is it possible to satisfy Eq. (7)? In Table 8 we list $(R_{eff})_M = e^{-gI_mL}$, using the values of g from columns 8 and 9 of Table 6. Unfortunately, no one presently knows how to make an edge treatment with an effective reflectivity less than about 10^{-3}. This means that unless the laser drive intensity is lower for long pulses, I_{SRS} from waves A, B, maybe D, E, G and H, will grow to some extent during the multiple traversals. If the long-pulse intensity is significantly lower than the short-pulse intensity, the necessity of satisfying Eq. (7) is relaxed.

The Bottom Line: Potential Performance Penalties on Nova/Novette

Having now introduced the basic features of the single- and multiple-traversal regimes, we next analyze quantitatively the seriousness of this situation for Nova/Novette.

The plans for Nova and Novette arrays are different. In the Novette baseline, Type II second-harmonic generation (SHG) is to be performed using a 5x5 array (15 cm crystals) one arm and a 3x3 array (27 cm array) on the other arm. Later, a pair of different arrays may be installed on each beam line to perform quadrature SHG and third-harmonic generation (THG). The Nova baseline design is quadrature SHG, and THG, using two arrays per beam.

The distinction between Type II SHG and quadrature SHG is important. The SRS gain coefficient for the 2ω wave is 0.21 cm/GW in the former configuration. However, in quadrature SHG, the strong 2ω wave that is generated in the first crystal has a coefficient of 0.43 cm/GW while it propagates through the second, rotated crystal. For calculations regarding quadrature SHG, we have assumed that 0.8 of the total 2ω output was generated in the first crystal.

A second distinction between Novette and Nova is the internal support structure. The first two arrays to be fielded on Novette during the next two or three months will have metal "eggcrates", and will perform Type II SHG. Further plans for installation on Novette of a quadrature-SHG/THG array are not firm at this time. Hence, it is not clear whether the

metal eggcrate would be retained in the Novette arrays beyond the initial Type II SHG phase. Nova plans for internal support structure are said to be wide open at present, and under consideration by others are corner bolts or pins or corner crosses or eggcrates, of materials yet to be specified.

The logic of the calculations that we have made to estimate the potential Nova/Novette performance limitations is shown in Fig. 7, and a sample printout in Fig. 8. From such computer runs, and with the criterion that not more than 1% of the incident pump intensity be allowed to side-scatter, we have calculated the maximum Nova/Novette (mean) intensity, for a variety of conditions, which could be propagated in KDP. In some cases, it is predicted that the Nova/Novette output cannot be reached without violating the 1% criterion. The 1% criterion was picked as a reasonable starting choice with regard to overall acceptable energy loss. In addition, for metal eggcrates, this criterion is safely below, by a factor of 2x or more, the measured damage threshold[11] for index-matching-fluid over aluminum metal.

It should be remembered (Argus, 1980) that if side-scattered fluence significantly above this damage threshold were allowed to occur, such that vaporization of a quantity of the fluid takes place, serious breakage of the array could follow.

Figure 9 is a legend for understanding the subsequent six figures 10-15, which are the major message of this report. We plot in Figs. 10-15 a single-cross-hatched band showing the present best estimate of performance limitations posed by SRS in KDP. We also show a pessimistic band (double cross-hatched). The expected SRS gain coefficient, which we will denote $\langle g \rangle$ (from Table 3), was used for the best-estimate band, and 1.5 $\langle g \rangle$, which is the upper end of the uncertainty range in g, was used for the pessimistic band. A result of all our calculations is that if the true gain coefficient is 50% less than expected, then SRS in KDP is predicted to not interfere with the baseline performance at ω, 2ω, or 3ω on Nova/Novette. In other words, if $g \leq .5 \langle g \rangle$, there may be no problem for Nova/Novette.

The reason the bands in Figs. 10-15 are bands instead of single curves is that two secondary uncertainties are included in these results--the effective edge reflectivity R and the spontaneous Raman noise intensity I_{s0}. These are secondary uncertainties because the SRS intensity varies linearly with them, as opposed to g with which the variation is exponential. In each band in Figs. 10-15, its lower edge is pessimistic (we used I_{s0} = 0.1 W/cm^2 and R = 90% for metal or R = 1% for absorbing glass) and its upper edge is optimistic (we used I_{s0} = 0.01 W/cm^2 and R = 50% for metal or R = 0.5% for absorbing glass were used). So the vertical width of a band shows the sensitivity to R and I_{s0}, while band-to-band comparison shows the sensitivity to the gain coefficient g.

The discontinuous changes on the edges of the bands in Figs. 9-15 occur primarily because of the discontinuous changes in SRS intensity that occur upon reflection at the KDP edge, occurring in multiples of 1.35 ns (for 27-cm KDP) and 0.75 ns (for 15-cm KDP). A secondary source of noise in the bands is the step size in our calculations to determine the safe output energy at each pulse duration. The bands in this report are for the purpose of indicating general features; high-precision calculations are not worthwhile at this point in time.

Novette 2ω

In Figure 10 we predict that, with the metal eggcrate, if g = 1.5 <g> then the Novette (Type II SHG) 2ω output will have to be reduced up to ~25% between 1 and 5 ns. For example, at 2.5 ns (with g = 1.5 <g>), if it were attempted to run Novette at its full baseline energy, calculations indicate that between 5% and 100% of the 2ω energy would be side-scattered into the metal eggcrate. If g $\leq$ <g>, then we predict no reduction in Novette 2ω will be necessary.

Figure 11 illustrates that, even if g were 50% larger than <g>, if absorbing glass partitions[12] (AGP) were used in the Novette arrays to separate the crystals, no SRS problem should be encountered. The AGP

could be in the form of an eggcrate or individual thin (few millimeters) strips. J. Williams has contacted suppliers regarding suitable ceramic/glass materials for absorbing glass members.

Nova 2ω

Next we look in Fig. 12 at Nova quadrature SHG. As mentioned earlier, Nova 2ω is not presently committed to metal eggcrates. Nevertheless, Fig. 12 was run with metal-eggcrate parameters to make the point that, depending on g, a metal eggcrate may indeed not be a viable design. Unless g is 50% of <g>, or less, our calculations indicate a problem. For comparison, Fig. 13 shows that absorbing glass partitions allow g to be almost as large as we anticipate without limiting the 2ω output.

Nova 3ω

The situation for Nova (or Novette) 3ω is shown in Figs. 14 and 15. Statements similar to those just made for quadrature 2ω apply. But, if g is as large as we estimate, the crystal segments must be small (15, not 27 cm), and an edge treatment such as AGP must be used in order to escape a performance penalty.

Ramifications for Optically-Non-Partitioned Arrays

The results presented in this report do not categorically rule out the possibility for optically non-partitioned arrays, by which we mean arrays with no opaque structures (except perhaps small corner pins, etc.) separating the crystal segments. Included in this performance category, in the limit of zero internal structure, would be 74-cm or larger single-crystal devices.

The reason such a large path length in the exponent of Eq. 4 is not sudden death is that Nova/Novette output fluence is rather independent of

pulse duration. The SRS gain term really depends on fluence F, not intensity, due to our transverse geometry:

$$e^{gI_m L_{eff}} = e^{gI_m c\tau/n} = e^{gFc/n} . \qquad (8)$$

So true constant-fluence output would yield aperture-independent SRS behavior, to first order. (In second-order, solid-angle/mode-count considerations in the effective spontaneous noise source would need to be considered).

Another way to think about this aspect is the following. For the metal eggcrate, if the metal were a 100% and perfectly-specular reflector, then the SRS evolution back-and-forth in a small segment would be the same as in a single larger crystal with no reflections: a 100% reflection reverses $\vec{k}$ but does not reduce the amplitude. So one doesn't expect the full-clear-aperture array to be radically different from the metal-eggcrate calculations, which used a 90% reflectivity, presented earlier. Fig. 16, for a hypothetical single-crystal, 74-cm quadrature doubler, confirms this notion. The performance penalty in Fig. 16 is essentially the same as for the metal-eggcrate 27-cm or 15-cm array shown in Fig. 12.

The point here is that if g is small enough to cause no problems for a metal-eggcrate array, then optically-non-partitioned arrays and/or larger single crystal devices may be viable. If g is not that small, then we have a physical limitation to the size of the crystal segments that we can employ. The utility of growing crystals beyond a certain size becomes moot.

We have predicted here that this certain size is in the ballpark of 27 cm; it remains to determine by measurement the true situation.

August 25, 1982

Section III. Plan for Measurements

We propose to instrument the 3x3 and 5x5 arrays on Novette to measure the side-scattered intensity on its initial 2ω shots later in this calendar year. This plan will protect Novette from any Raman-induced damage. This plan will enable us to measure in situ the SRS strength. We will then be in acceptable position to proceed with Nova arrays. We feel that the alternative of making small-beam measurements and scaling up the results numerically is unacceptably risky due to the geometry-sensitive noise source and the exponential penalty which comes from errors in measurement of the gain coefficient. In plain words, we are near the turn-on of an exponential problem and we had better know where that turn-on occurs.

The diagnostics needed on the Novette arrays are minor (fiber-optic cable ports and line-of-sight holes) and B. Johnson and J. Williams have already made provisions for them. W. L. Smith will be responsible for the actual measurements on Novette. Your comments are welcome.

// NOTE ADDED IN PRESS: We should mention that the largest gIL product (in KDP) generated anywhere, to our knowledge, was by G. Linford during 4ω work on Argus in 1981. Linford[a] extracted 6.3 GW/cm^2 ("e" wave) from KDP at 4ω. This gives a best-estimate gIL of .44 cm/GW x 6.3 GW/cm^2 x 8 cm = 22.2 which is as high as any of the single-traversal numbers in Table 6, columns 7-9. You will recall[b] that Linford reported an unexplained fast turn-on of nonlinear loss in that work. The turn-on was faster than easily accountable by two-photon absorption (2PA), and the 2PA coefficient extracted from the 4ω Argus work was larger by 1.7x to 17x than previously-reported values. Hence, it is possible that transverse stimulated Raman scattering took place in that work, and went undetected. Since no index-matching fluid was used in that work, side-scattered 4ω energy would not necessarily have destroyed the 4ω cell in the manner that is conceivable for fluid-filled cells.

(a) G. J. Linford, Laser Program Memo GL81-06, April 12, 1981.
(b) G. J. Linford, Laser Program Memo GL81-11, May 29, 1981.

References

1. W. Kaiser and M. Maier, in Laser Handbook, edited by F. T. Arrecchi and E. O. Schultz-Dubois, North-Holland, Amsterdam, 1972.
2. A. Penzkofer, A. Laubereau, and W. Kaiser, in Prog. Quant. Electr. Vol. 6, pp. 55-140, Pergamon Press, London (1979).
3. F. Aussenegg and U. Deserno, Opt. Commun. 2, 295 (1970).
4. M. J. Colles, Opt. Commun. 1, 169 (1969).
5. G. G. Bret and H. P. Weber, IEEE J. Quant. Electr. 4, 807 (1968).
6. J. B. Grun, A. K. McQuillan, and B. P. Stoicheff, Phys. Rev. 180, 61 (1969).
7. F. J. McClung, W. G. Wagner, and D. Weiner, Phys. Rev. Lett. 15, 96 (1965).
8. W. D. Johnston, Jr., I. P. Kaminow, and J. G. Bergman, Appl. Phys. Lett. 13, 190 (1968).
9. J. G. Skinner and W. G. Nilsen, J.O.S.A. 58, 113 (1968).
10. N. Bloembergen, G. Bret, and P. Lallemand, A. Price, and P. Simova, IEEE J. Quant. Electr. QE-3, 197 (1967).
11. J. Swain, Laser Damage Group Memo, 1981.
12. L. Smith, Laser R&D Memo UVM 82-16, July (1982).

Table 1. Literature values of stimulated Raman gain coefficient g for benzene 992 cm^{-1} vibrational mode.

Authors	pump λ (nm)	SRS g at pump λ (cm/GW)	SRS g at 488-nm pump (cm/GW)	Comments
Aussenegg et al.[3]	532.	5	5.5	estimate from measureme of stimulated Raman threshold
Colles[4]	532.	~5	~5.5	estimate from stimulate conversion of power to the Stokes frequency
Colles[4]	532.	5.2	5.7	computation from spontaneous data
Bret & Weber[5]	532.	4.5	4.9	" "
Brun et al.[6]	694.3	2.8	4.1	" "
McClung et al.[7]	694.3	3.8	5.5	" "
Johnston et al.[8]	1064.	2.7	6.3	" "
Skinner & Nilson[9]	694.3	3	4.4	" "

Table 2. Raman Scattering Results, Pump Laser = 488 nm (20,492 cm^{-1}) Argon.

A	B	C	D	E	F	G	H	J
Material	ω_R	ω_s	$\left(\frac{\omega_s \text{benzene}}{\omega_s}\right)^3$	Γ^*	$\frac{S}{S_{benzene}}$	$\frac{g}{g_{benzene}}$	$g_{absolute}$ for 488-nm pump	$g_{absolute}$ for 532-nm pump
	cm^{-1}	cm^{-1}		cm^{-1}			cm/GW	cm/GW
Benzene	992	19500	1.000	2.3	1.00	1.00	5.5	5.0
Nitrobenzene	1345	19147	1.056	6.6	0.96	1.01	5.5	5.0
Halocarbon 56	438	20054	0.920	**	0.020	0.018	0.10	0.092
Cargille 5610	998	19494	1.000	21.0	0.31	0.31	1.7	1.6
SiO_2 crystal	468	20024	0.934	8.0	0.099	0.093	0.51	0.47
KDP "e"	915	19576	0.989	20.0	0.043	0.042	0.23	0.21
KDP "o"	915	19576	0.989	20.0	0.085	0.084	0.46	0.42

*Linewidth Γ is included for information only and is not used in calculation of the gain parameters in columns G-J.

**~10 to 20 cm^{-1}, uncertain due to three overlapping vibrational lines.

Table 3. Stimulated Raman Gain Coefficient in KDP at Nova/Novette Wavelengths

Pump λ (nm)	Direction of Polarization in KDP	Pump ω (cm^{-1})	ω_s (cm^{-1})	λ_s (nm)	SRS g (cm/GW)
1053	"e"	9,497	8,582	1165	0.10
1053	"o"	9,497	8,582	1165	0.20
526.5	"e"	18,993	18,078	553	0.21
526.5	"o"	18,993	18,078	553	0.43
351	"e"	28,490	27,575	363	0.33
351	"o"	28,490	27,575	363	0.65

Table 4. Stimulated Raman Gain Coefficient in Halocarbon 56 fluid at Nova/Novette Wavelengths.

Pump λ (nm)	Pump ω (cm^{-1})	ω_s (cm^{-1})	ω_s (nm)	SRS g (cm/GW)
1053	9,497	9,059	1104	0.046
526.5	18,993	18,555	539	0.095
351	28,490	28,052	356	0.14

Table 5. Nova Maximum Output Intensity (GW/cm^2) Versus Pulse Duration

Pulse Duration (ns)	ω	$2\omega^*$	$3\omega^*$
0.5	4.03	3.60	3.17
1.0	3.26	2.80	2.68
1.5	2.76	2.33	2.25
2.0	2.28	1.87	1.87
2.5	1.88	1.50	1.52
3.0	1.62	1.22	1.27
3.5	1.40	1.00	1.08
4.0	1.24	0.84	0.88
4.5	1.11	0.75	0.72
5.0	1.00	0.60	0.59

*Doubler and tripler thickness is 1 cm.

Table 6. Short-Pulse Parameters for Stimulated Raman Scattering in 27-cm and 15-cm KDP Segments at Nova Intensity Levels. In this pulse-duration range, SRS is limited to ≦ 1 traversal of the KDP segment.

Column	1	2	3	4	5	6	7	8	9
	WAVE	ORIENTATION	NOVA MAX INTENSITY I_m inside KDP (GW/cm^2)			SRS g (cm/GW)	gI_mL_{eff}		
			1.0 ns	1.35 ns	0.75 ns		1.0 ns L_{eff}=20 cm	1.35 ns L_{eff}=27 cm	0.75 ns L_{eff}= 15 cm
A.	ω in Type I SHG	"o"	3.2	2.9	3.6	0.20	12.8	15.7	10.8
B.	2ω in Type I SHG	"e"	2.8	2.6	3.1	0.21	11.8	14.7	9.8
C.	Half the ω in Type II SHG	"e"	1.6	1.3	1.8	0.10	3.2	3.5	2.7
D.	Half the ω in Type II SHG	"o"	1.6	1.3	1.8	0.20	6.4	7.0	5.4
E.	2ω in Type II SHG	"e"	2.8	2.6	3.1	0.21	11.8	14.7	9.8
F.	ω in Type II THG	"e"	1.1	1.0	1.2	0.10	2.2	2.7	1.8
G.	2ω in Type II THG	"o"	2.1	1.9	2.4	0.43	18.1	22.1	15.5
H.	3ω in Type II THG	"e"	2.7	2.35	2.9	0.33	17.8	20.9	14.4

Table 7. Range of spontaneous Raman noise intensity I_{s0} and corresponding gI_mL_{eff} necessary to generate 0.1 GW/cm^2 at the Stokes frequency.

I_{s0} (W/cm^2)	gI_mL_{eff} to generate I_{SRS}=0.1 GW/cm^2
.001	25.3
.01	23.0
.1	20.7

Table 8. Maximum Allowable Effective Reflectivity

$(R_{eff})_m$ to satisfy $R_{eff} \leqq e^{gI_mL}$

WAVE	$(R_{eff})_m$	
	L_{eff} = 27 cm*	L_{eff} = 15 cm**
A	1×10^{-7}	2×10^{-5}
B	4×10^{-7}	5×10^{-5}
C	3×10^{-2}	0.06
D	9×10^{-4}	4×10^{-3}
E	4×10^{-7}	5×10^{-5}
F	7×10^{-2}	0.16
G	2×10^{-10}	1×10^{-7}
H	8×10^{-10}	5×10^{-7}

*gI_mL_{eff} values are from Table 6, column 8, for 1.35 ns.

**gI_mL_{eff} values are from Table 6, column 9, for 0.75 ns.

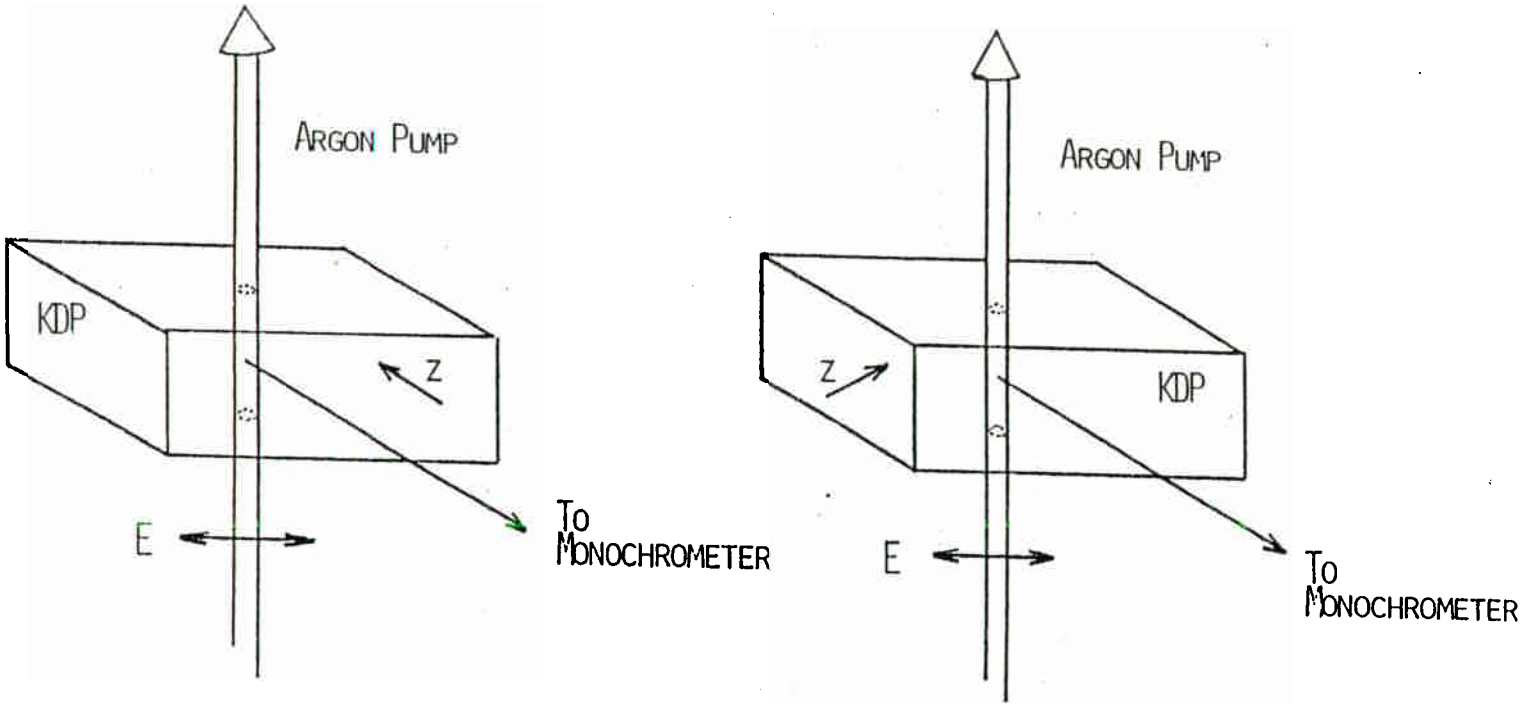

ORIENTATION "E"

ORIENTATION "O"

FIG. 1 SPONTANEOUS RAMAN SCATTERING MEASUREMENT GEOMETRY

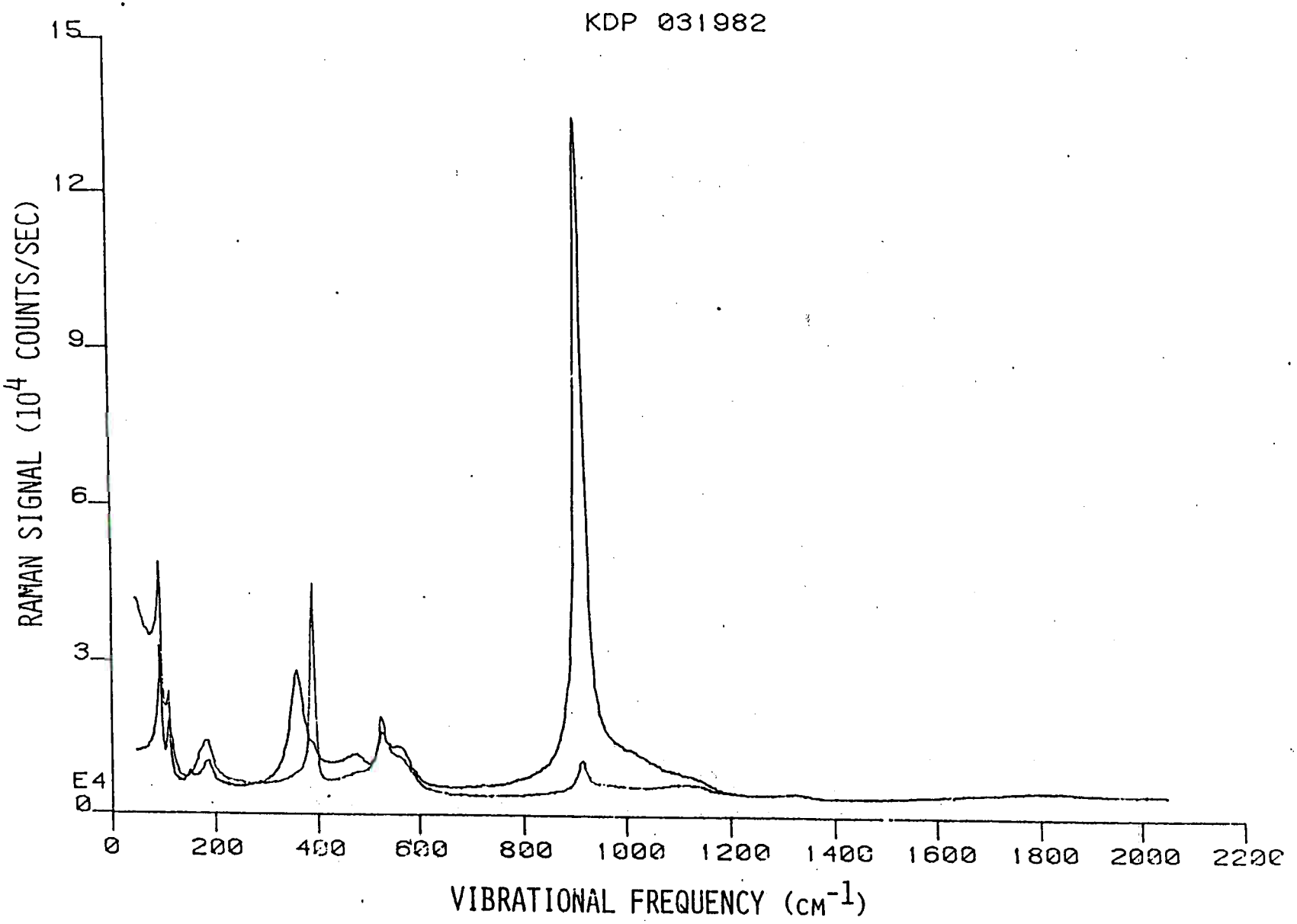

FIG. 2: RAMAN SPECTRUM OF KDP. BOTH THE "POLARIZED" AND "DEPOLARIZED" SPECTRA ARE SHOWN. THE STRONG PEAK AT 915 cm^{-1} IS DUE TO A VIBRATION IN THE PO_4 NETWORK OF KDP.

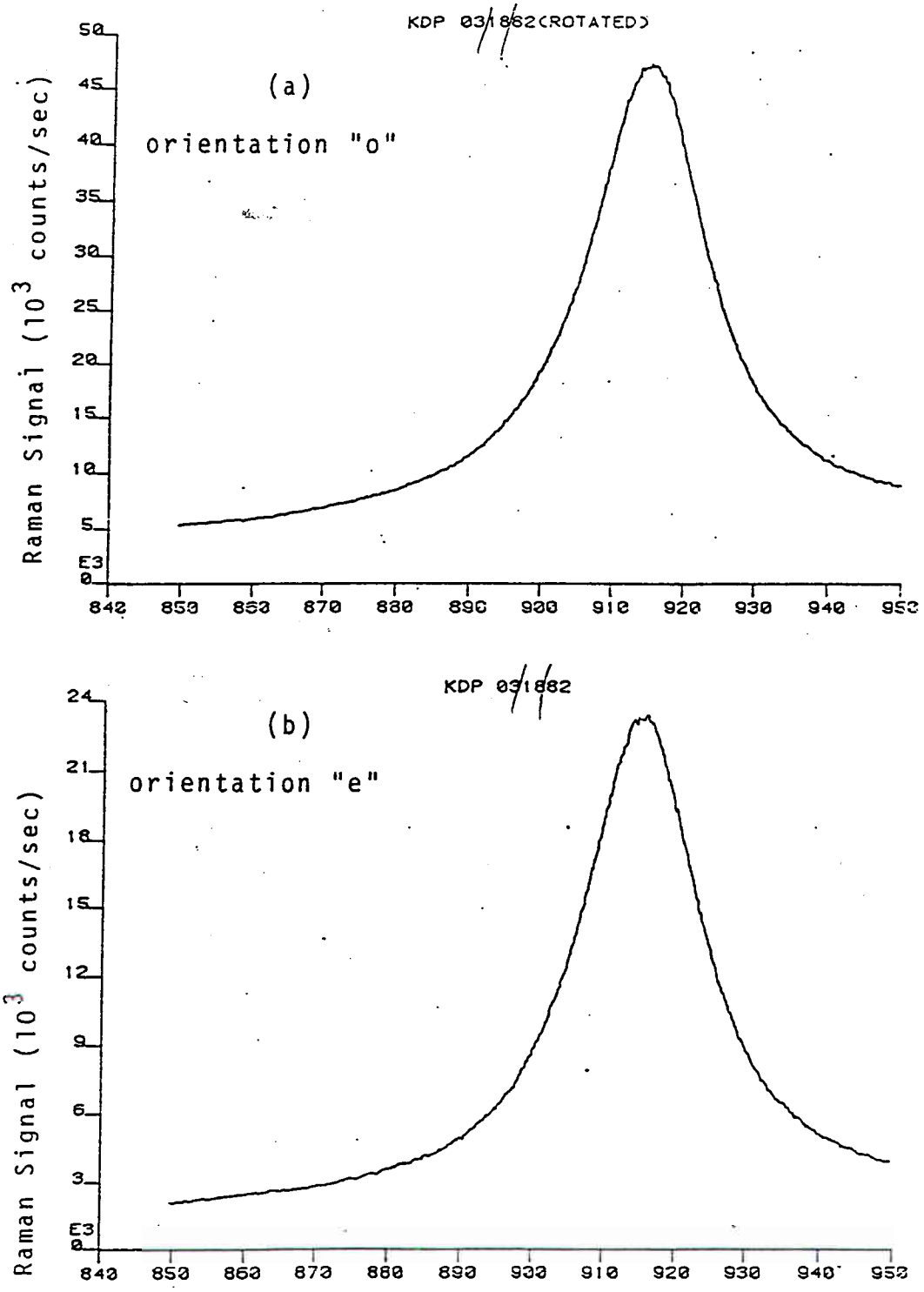

Fig. 3: Strong Raman peak at 915 cm^{-1} in KDP.

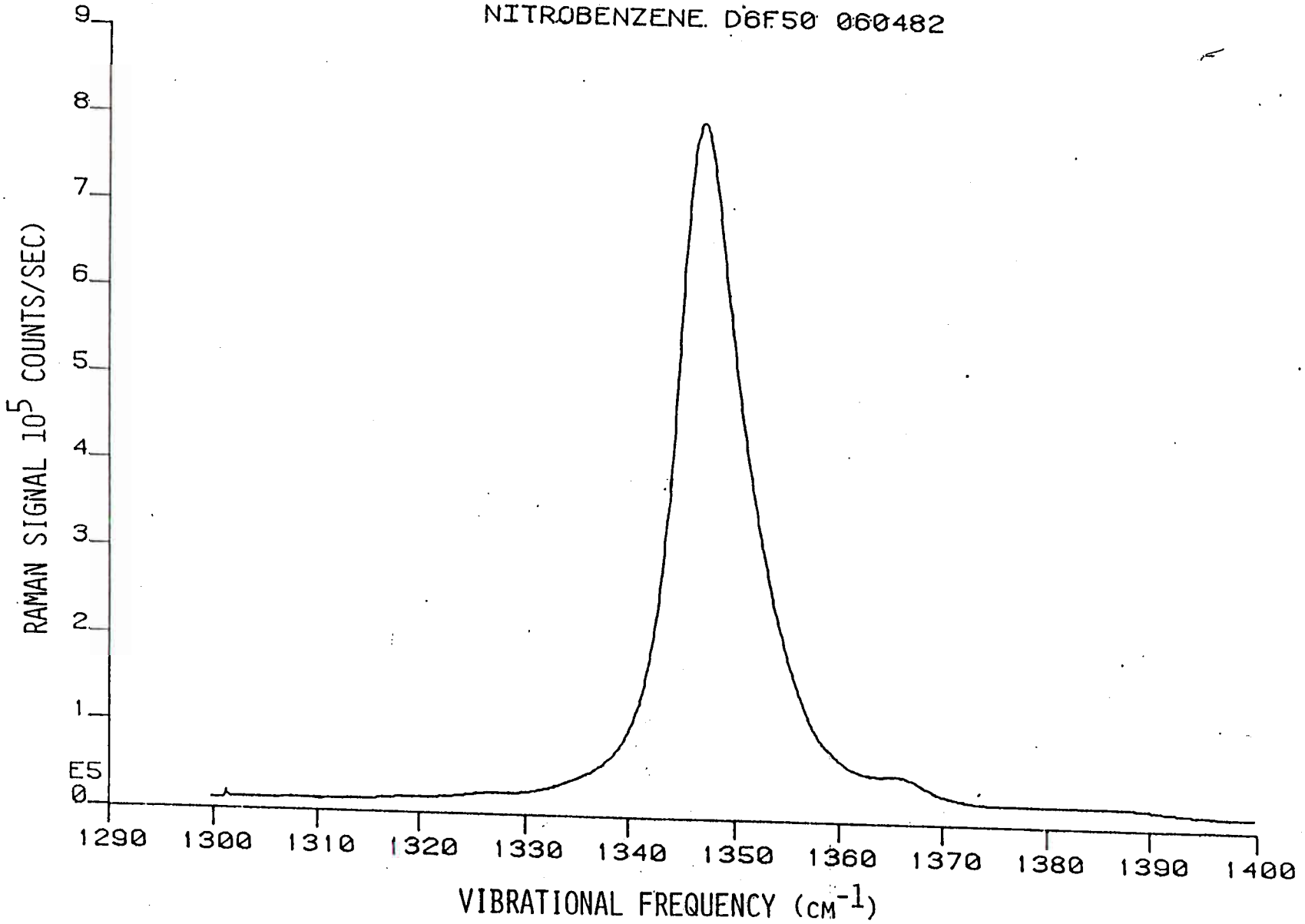

FIG. 4: STRONG RAMAN PEAK AT 1350 cm^{-1} IN NITROBENZENE

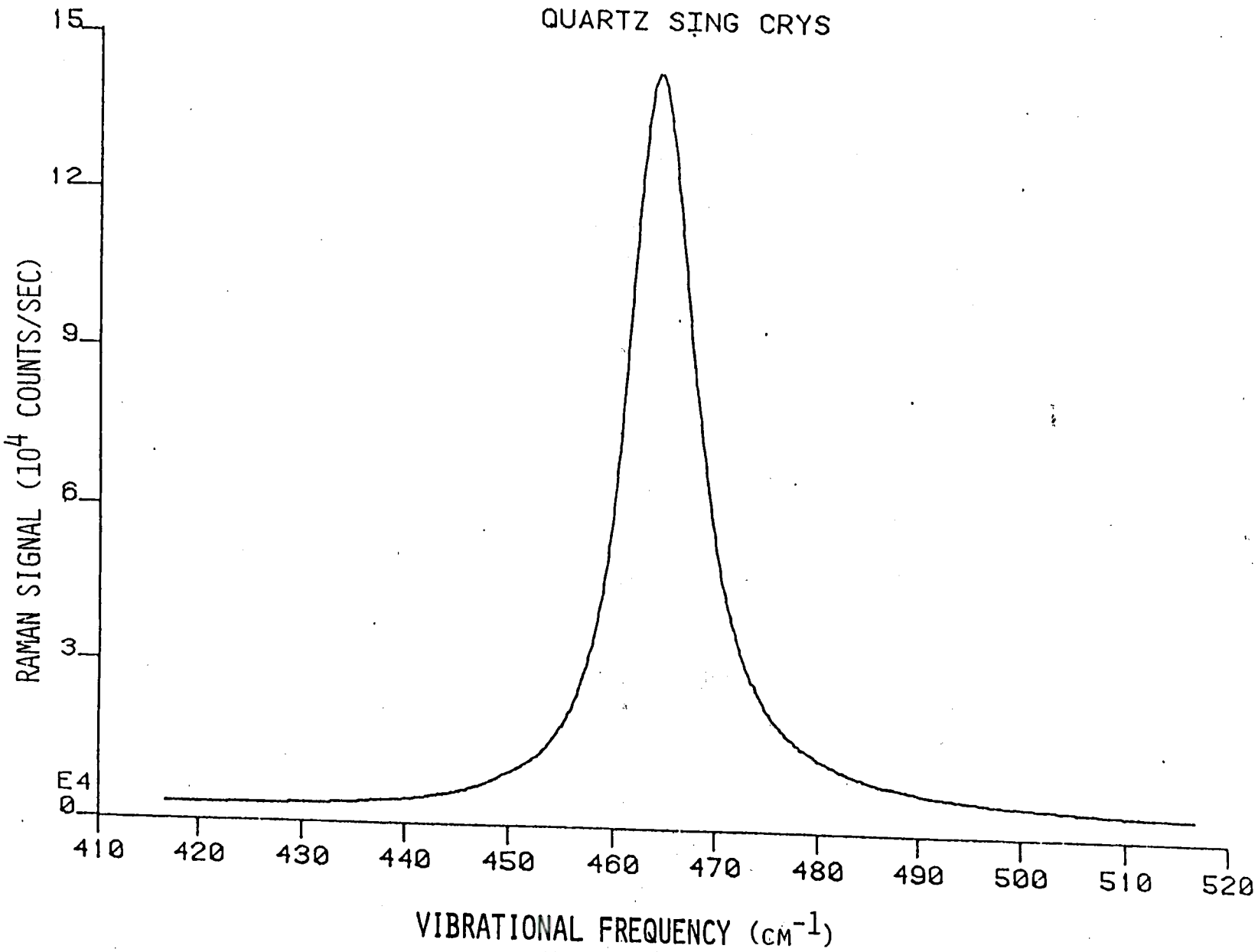

FIG. 5: STRONG RAMAN PEAK AT 465 cm^{-1} IN CRYSTALLINE QUARTZ

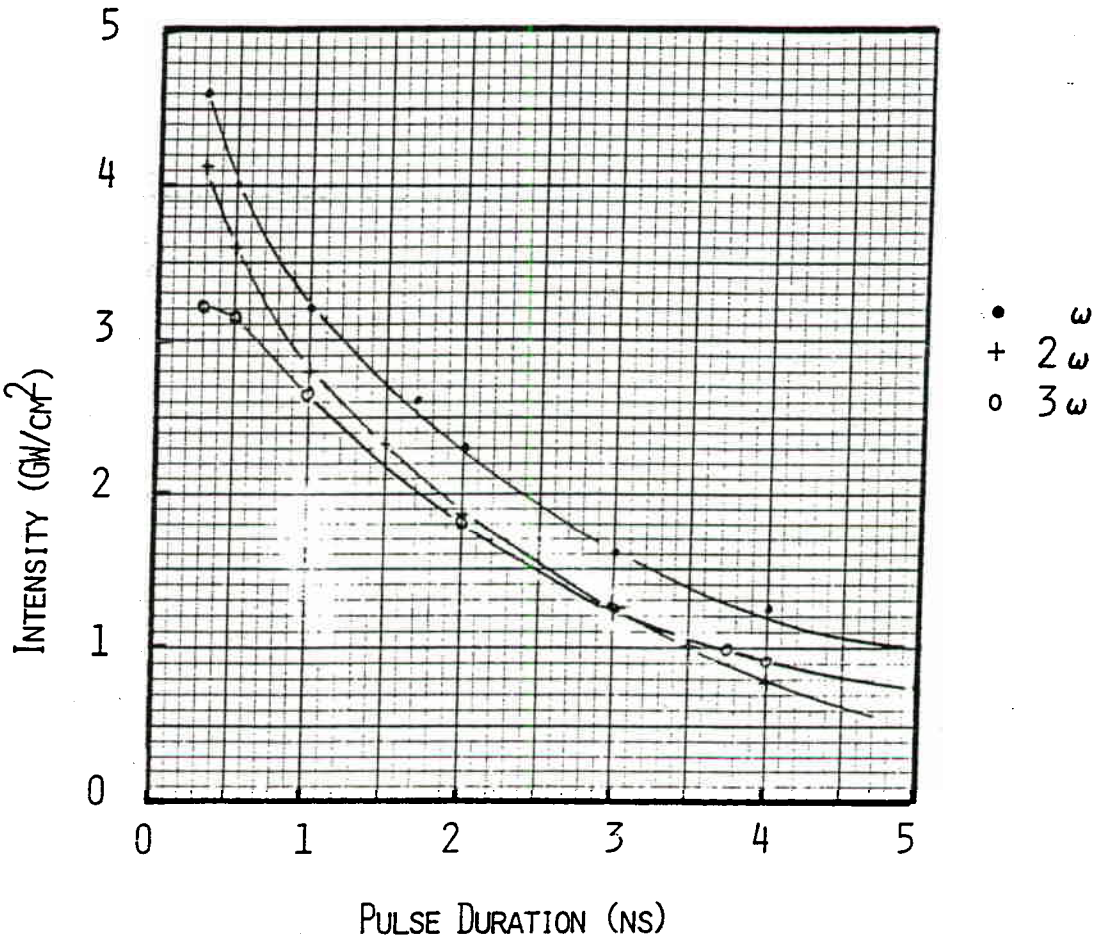

FIG. 6 NOVA MAXIMUM INTENSITY (MEAN) VERSUS PULSE DURATION

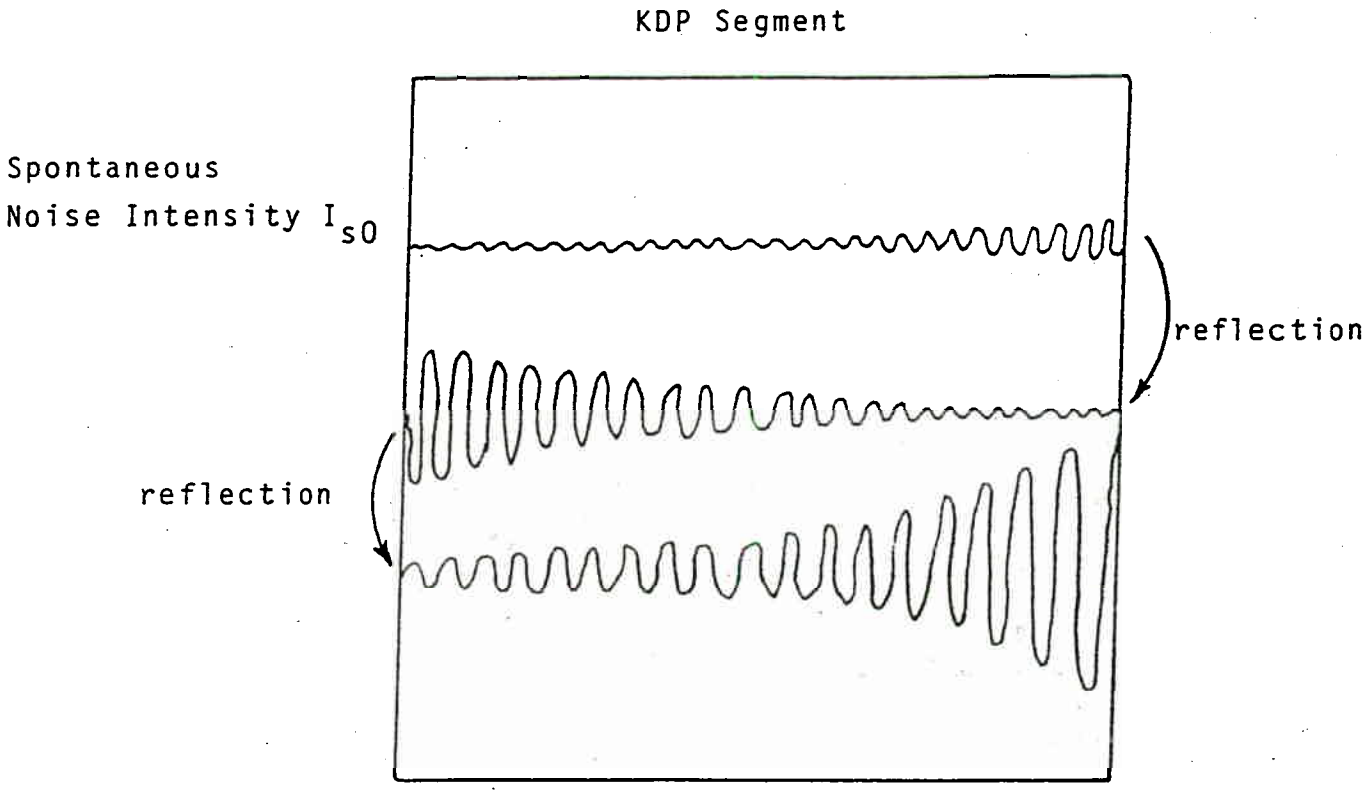

Fig. 7: Schematic of SRS calculation showing the temporal evolution of the SRS intensity when there is net SRS growth.

WAVE =	2 OMEGA IN END GAIN RATE (1/ns)
SRS GAIN COEFFICIENT (cm/GW) =	0.43
KDP CRYSTAL SIZE (cm) =	27
R1,R2,R3:	90 50 10

Duration (ns)	Intensity (GW/cm^2)	SRS INTENSITY (W/cm2) SCATTERED TRANSVERSELY BY CRYSTAL								
		I_{s0} (W/cm^2) /	0.1		0.01			0.001		
		R(%) /	90	50	10	90	50	10	90	50	10
.5	2.88		2.4E+04	2.4E+04	2.4E+04	2.4E+03	2.4E+03	2.4E+03	2.4E+02	2.4E+02	2.4E+02
.8	2.52		1.1E+06	1.1E+06	1.1E+06	1.1E+05	1.1E+05	1.1E+05	1.1E+04	1.1E+04	1.1E+04
1.0	2.24		2.3E+07	2.3E+07	2.3E+07	2.3E+06	2.3E+06	2.3E+06	2.3E+05	2.3E+05	2.3E+05
1.5	1.86		2.4E+09	1.3E+09	2.6E+08	2.4E+08	1.3E+08	2.6E+07	2.4E+07	1.3E+07	2.6E+06
2.0	1.50		1.4E+10	8.0E+09	1.6E+09	1.4E+09	8.0E+08	1.6E+08	1.4E+08	8.0E+07	1.6E+07
2.5	1.20		1.4E+10	8.0E+09	1.6E+09	1.4E+09	8.0E+08	1.6E+08	1.4E+08	8.0E+07	1.6E+07
3.0	.98		7.7E+09	2.4E+09	9.6E+07	7.7E+08	2.4E+08	9.6E+06	7.7E+07	2.4E+07	9.6E+05
3.5	.80		2.3E+09	7.2E+08	2.9E+07	2.3E+08	7.2E+07	2.9E+06	2.3E+07	7.2E+06	2.9E+05
4.0	.67		8.3E+08	2.6E+08	1.0E+07	8.3E+07	2.6E+07	1.0E+06	8.3E+06	2.6E+06	1.0E+05
4.5	.60		8.9E+08	1.5E+08	1.2E+06	8.9E+07	1.5E+07	1.2E+05	8.9E+06	1.5E+06	1.2E+04
5.0	.48		6.7E+07	1.2E+07	9.2E+04	6.7E+06	1.2E+06	9.2E+03	6.7E+05	1.2E+05	9.2E+02
		FRACTION OF INCIDENT INTENSITY SCATTERED BY SRS								
.5	2.88		8.3E-06	8.3E-06	8.3E-06	8.3E-07	8.3E-07	8.3E-07	8.3E-08	8.3E-08	8.3E-08
.8	2.52		4.5E-04	4.5E-04	4.5E-04	4.5E-05	4.5E-05	4.5E-05	4.5E-06	4.5E-06	4.5E-06
1.0	2.24		1.0E-02	1.0E-02	1.0E-02	1.0E-03	1.0E-03	1.0E-03	1.0E-04	1.0E-04	1.0E-04
1.5	1.86		1.0E+00	7.1E-01	1.4E-01	1.3E-01	7.1E-02	1.4E-02	1.3E-02	7.1E-03	1.4E-03
2.0	1.50		1.0E+00	1.0E+00	1.0E+00	9.6E-01	5.3E-01	1.1E-01	9.6E-02	5.3E-02	1.1E-02
2.5	1.20		1.0E+00	1.0E+00	1.0E+00	1.0E+00	6.7E-01	1.3E-01	1.2E-01	6.7E-02	1.3E-02
3.0	.98		1.0E+00	1.0E+00	9.8E-02	7.9E-01	2.4E-01	9.8E-03	7.9E-02	2.4E-02	9.8E-04
3.5	.80		1.0E+00	9.0E-01	3.6E-02	2.9E-01	9.0E-02	3.6E-03	2.9E-02	9.0E-03	3.6E-04
4.0	.67		1.0E+00	3.8E-01	1.5E-02	1.2E-01	3.8E-02	1.5E-03	1.2E-02	3.8E-03	1.5E-04
4.5	.60		1.0E+00	2.5E-01	2.0E-03	1.5E-01	2.5E-02	2.0E-04	1.5E-02	2.5E-03	2.0E-05
5.0	.48		1.4E-01	2.4E-02	1.9E-04	1.4E-02	2.4E-03	1.9E-05	1.4E-03	2.4E-04	1.9E-06

Fig. 8. Example of calculated results. The encircled region shows the range of intensity, noise intensity I_{s0}, and reflectivity R which cause more than 1% of the incident intensity to be side-scattered.

LEGEND FOR FIGURES 10 - 16

THE UNCERTAINTY IN THE SRS GAIN COEFFICIENT $\langle g \rangle$ IS $\pm$ 50%

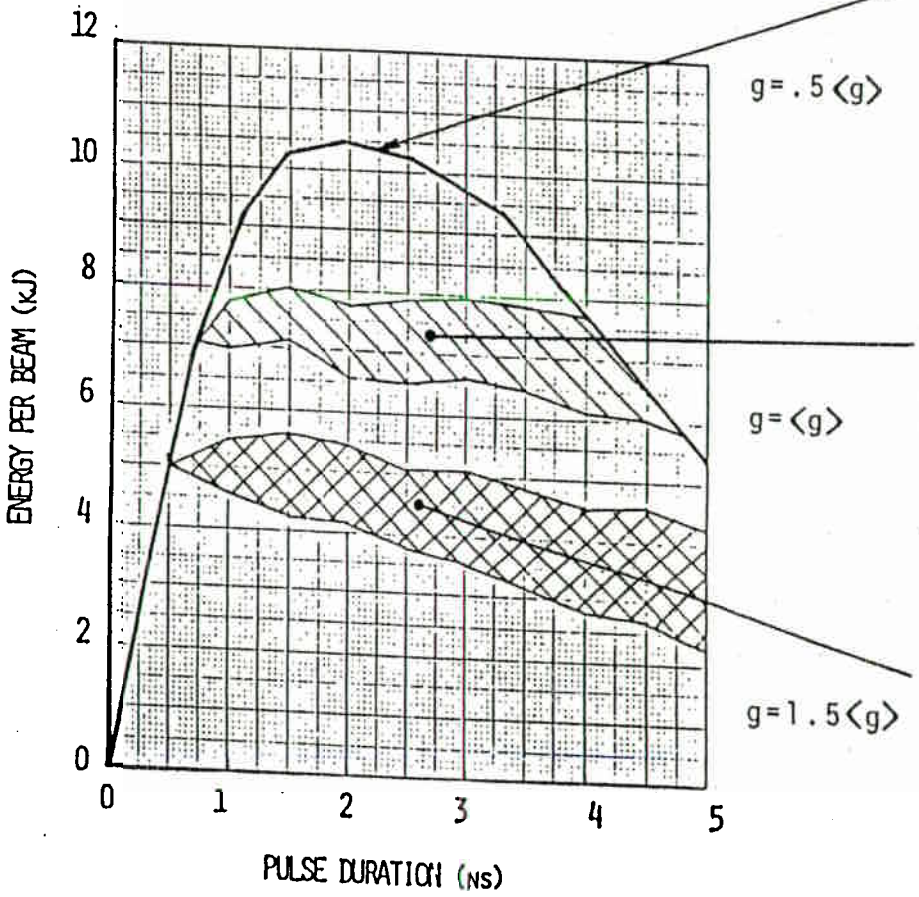

SOLID CURVE IS THE NOVA/NOVETTE BASELINE OF ENERGY VERSUS PULSE DURATION. IF THE ACTUAL SRS GAIN COEFFICIENT IS 50% LESS THAN EXPECTED, OUR RESULTS INDICATE THAT SRS WILL NOT INTERFERE WITH THIS BASELINE PERFORMANCE.

PREDICTED REGION INTO WHICH THE BASELINE PERFORMANCE WILL DROP USING BEST AVAILABLE DATA FOR SRS, AND USING THE CRITERION THAT NOT MORE THAN 1% OF THE INCIDENT INTENSITY BE ALLOWED TO SIDE-SCATTER.

PREDICTED REGION INTO WHICH THE BASELINE PERFORMANCE WILL DROP IF THE ACTUAL SRS GAIN COEFFICIENT IS 50% LARGER THAN OUR BEST ESTIMATE.

FIG. 9

LEGEND

POTENTIAL REDUCTION IN NOVETTE 2ω OUTPUT DUE TO SRS IN KDP

WITH PRESENT METAL EGGCRATE

27-cm KDP

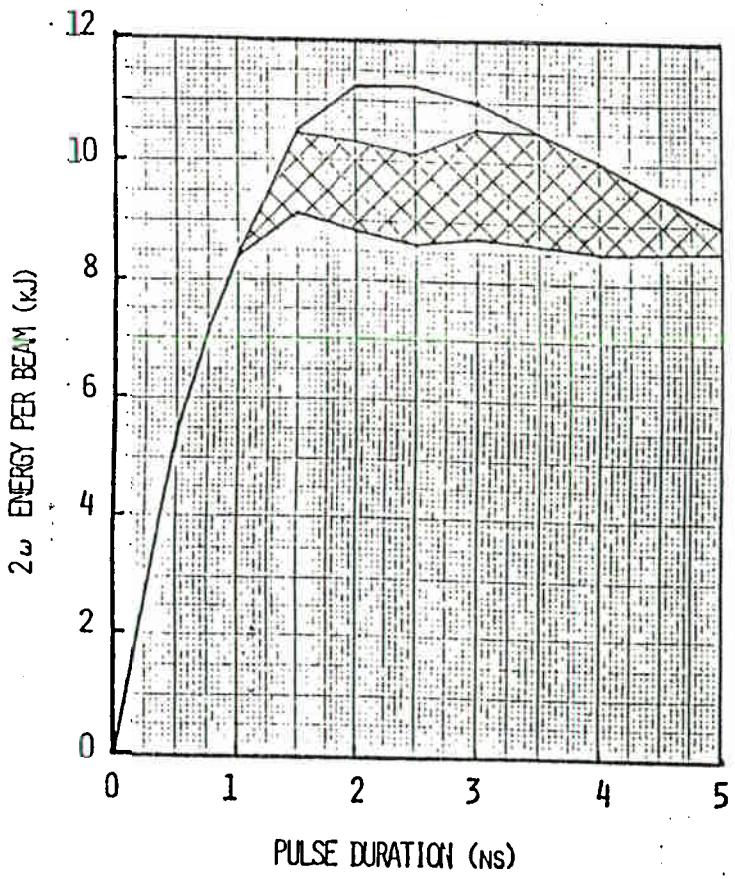

15-cm KDP

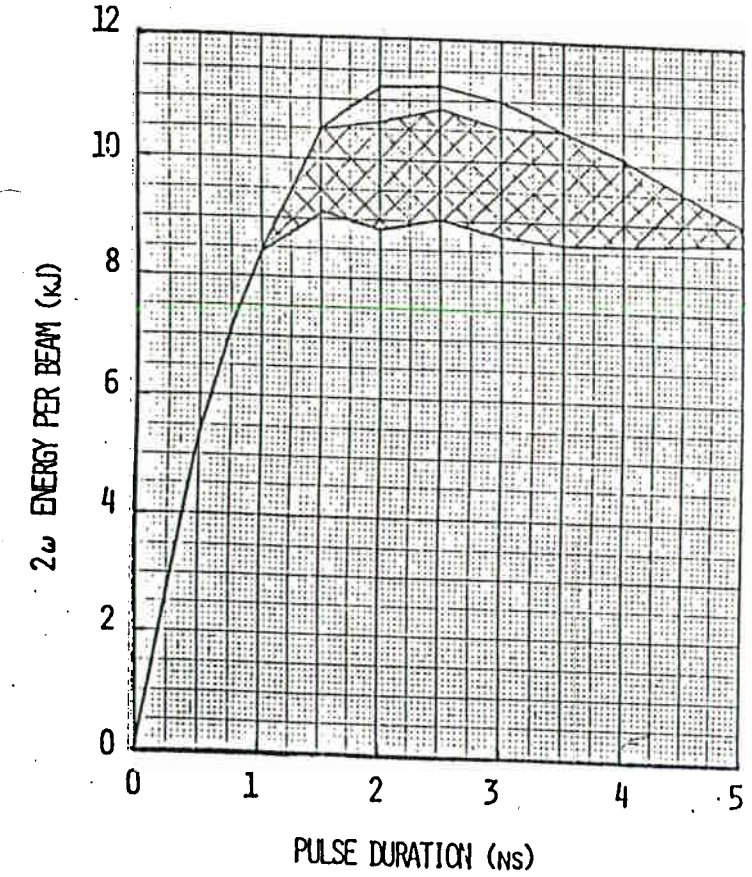

WITH AGP, NO REDUCTION IN NOVETTE 2ω OUTPUT IS PREDICTED

WITH ABSORBING GLASS PARTITIONS (AGP)

27-CM KDP

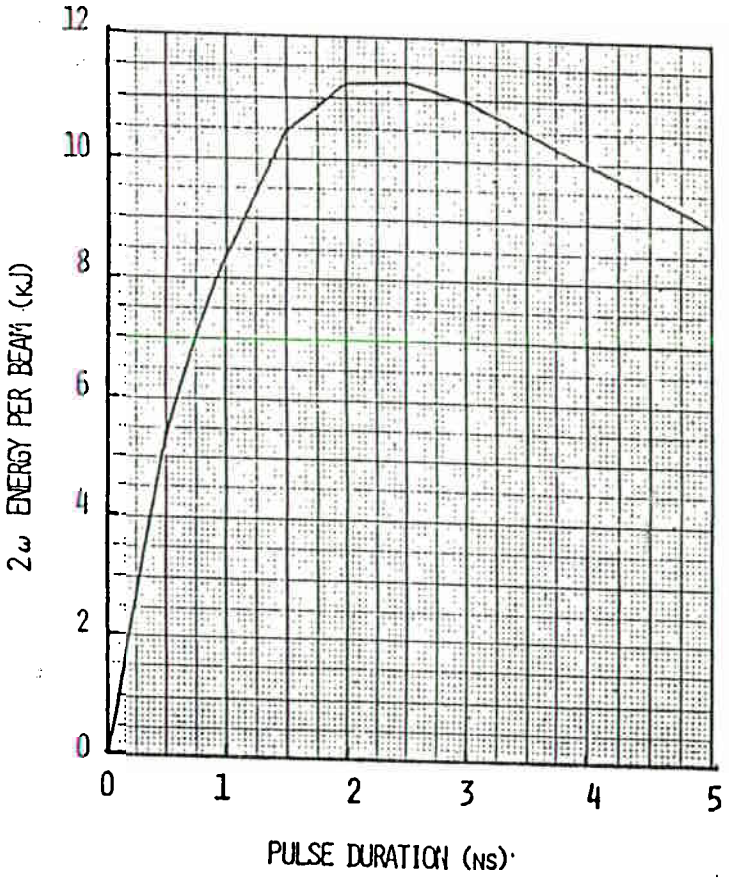

15-CM KDP

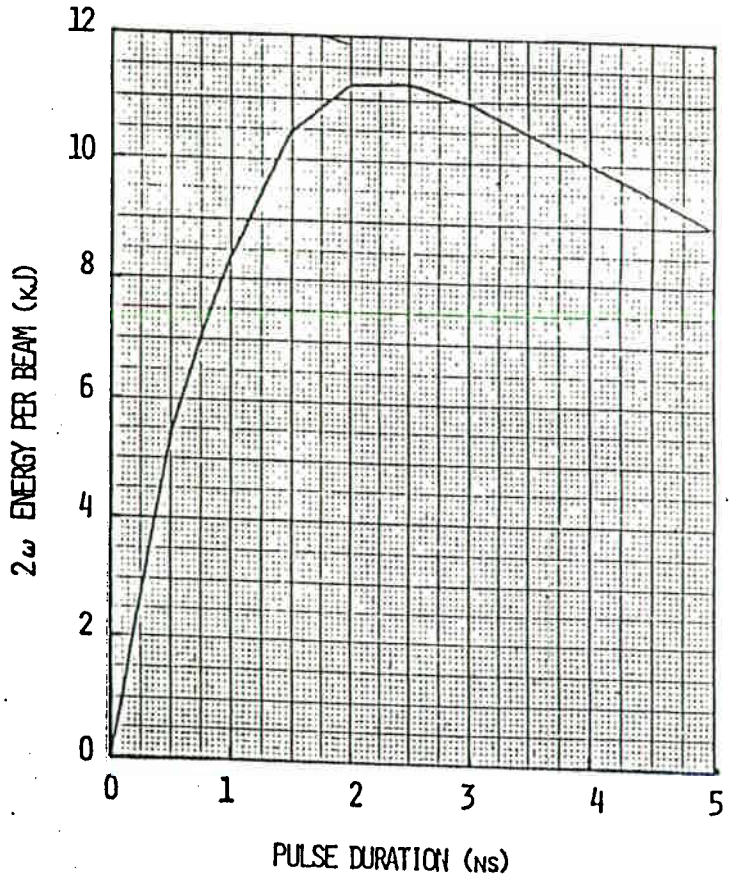

POTENTIAL REDUCTION IN NOVA 2ω OUTPUT DUE TO SRS IN KDP

WITH PRESENT METAL EGGCRATE

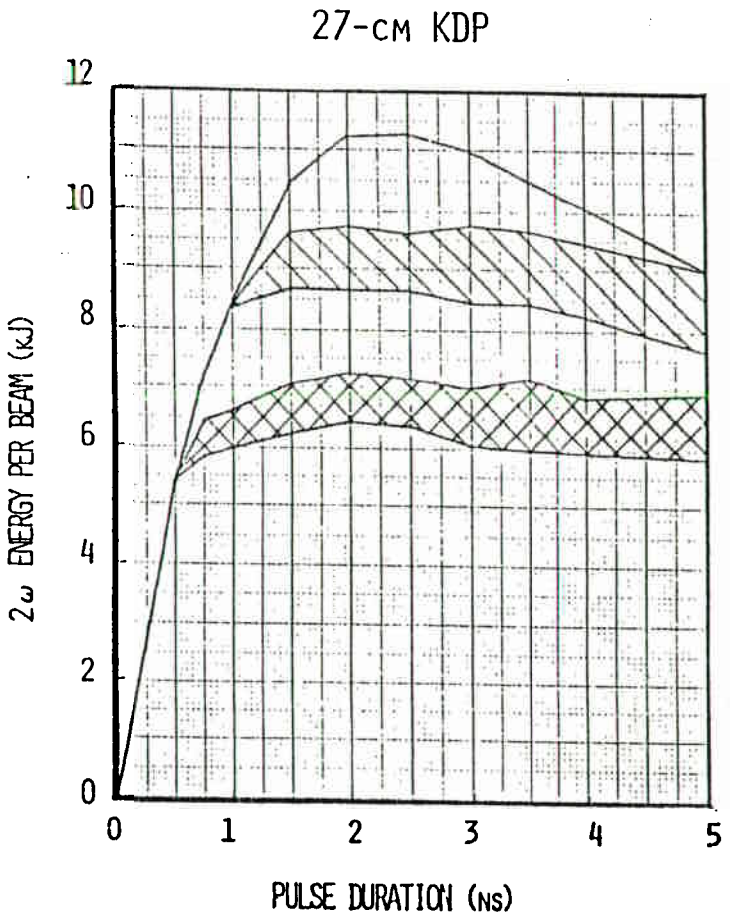

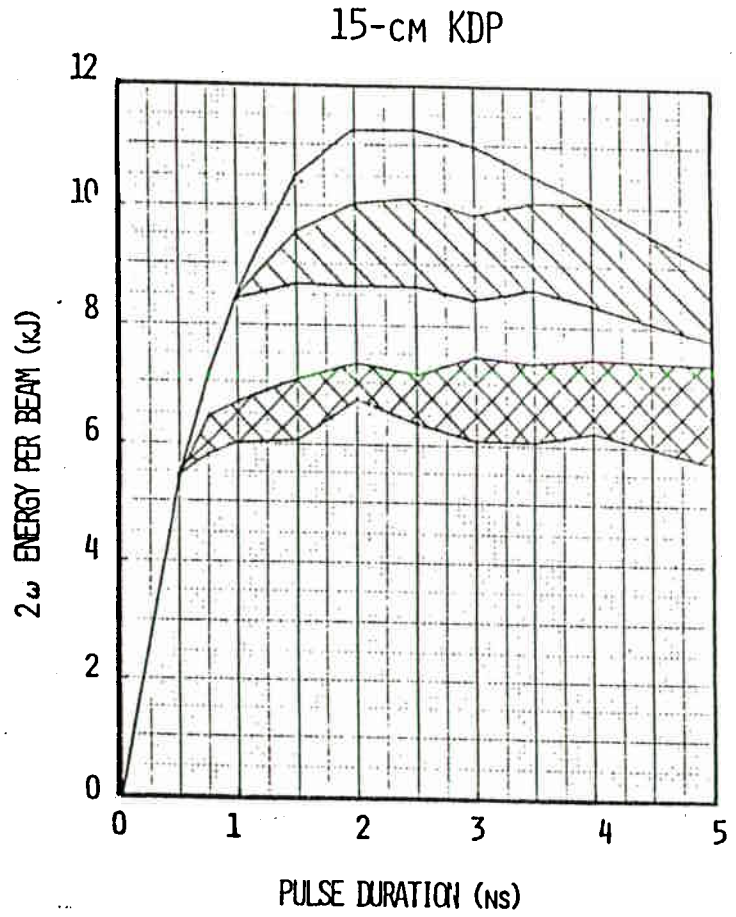

FIG. 12

LESS REDUCTION IN NOVA 2ω OUTPUT IS NEEDED WITH AGP

WITH ABSORBING GLASS PARTITIONS (AGP)

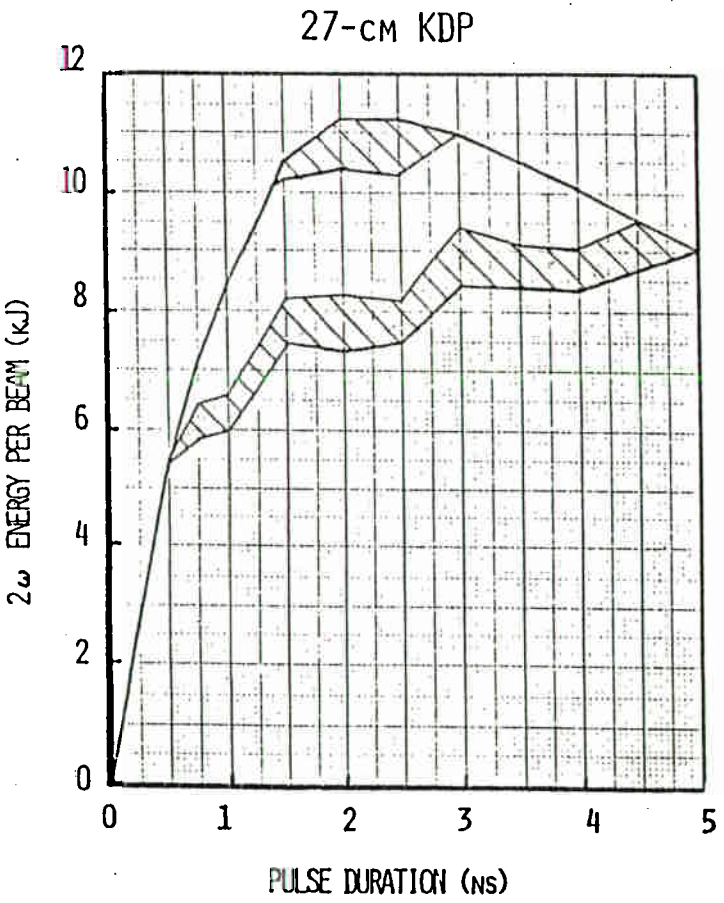

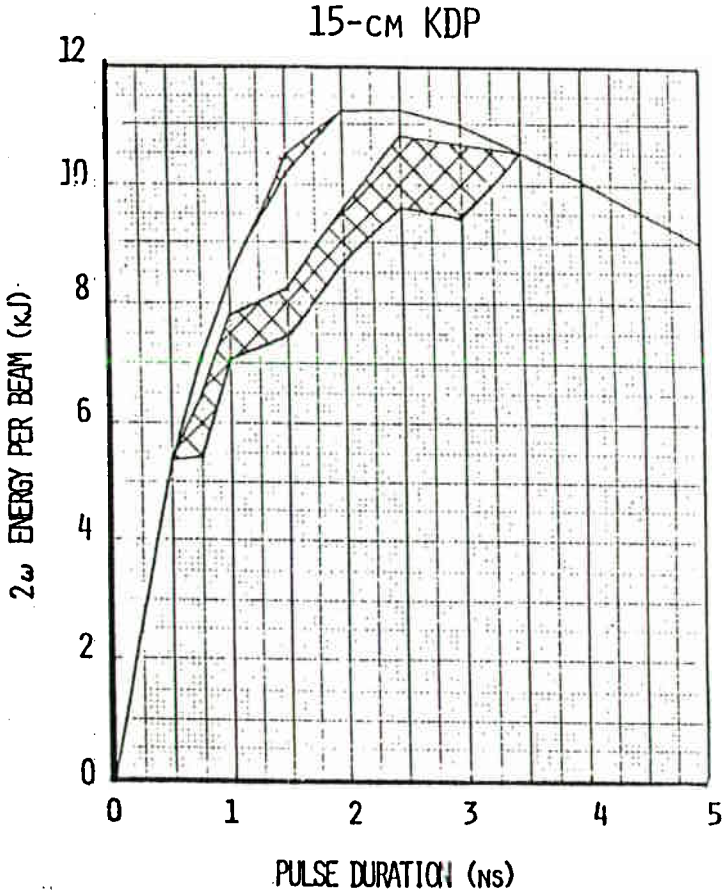

POTENTIAL REDUCTION IN NOVA 3ω OUTPUT DUE TO SRS IN KDP

WITH PRESENT METAL EGGCRATE

27-cm KDP

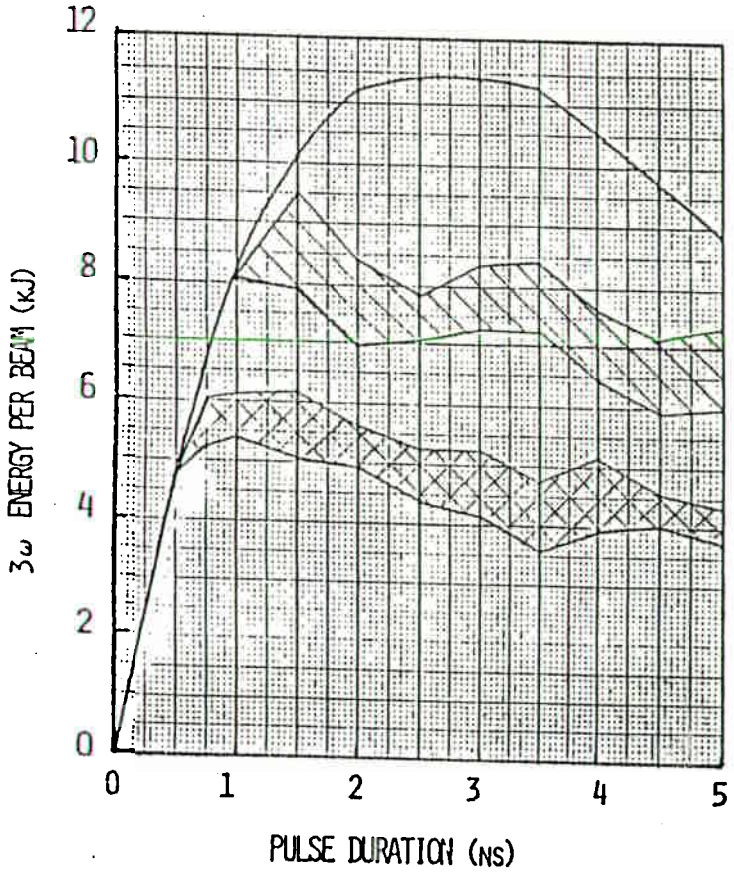

15-cm KDP

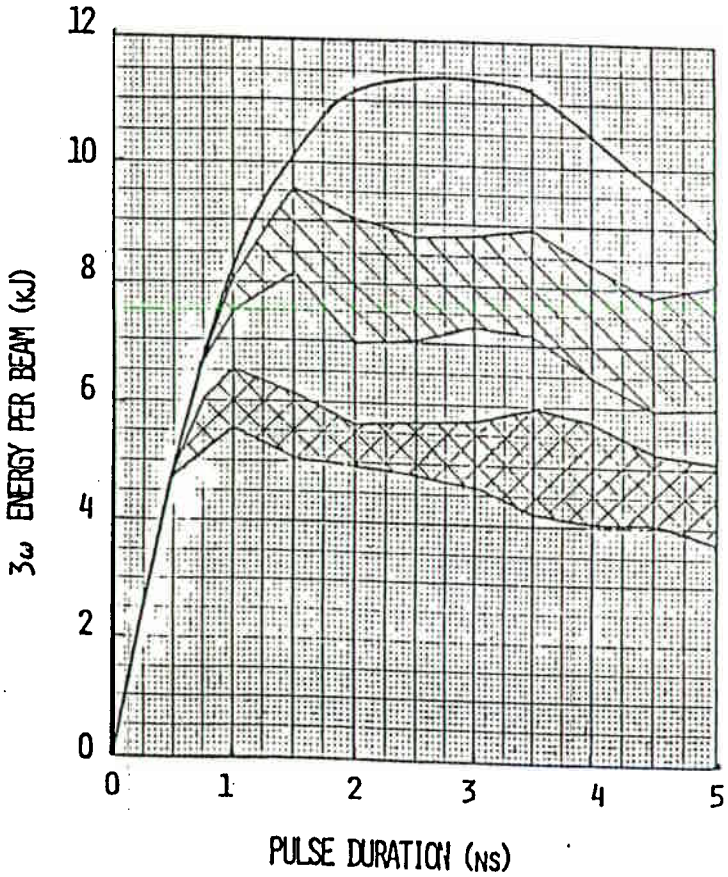

LESS REDUCTION IN NOVA 3ω OUTPUT IS NEEDED WITH AGP

WITH ABSORBING GLASS PARTITIONS (AGP)

27-cm KDP

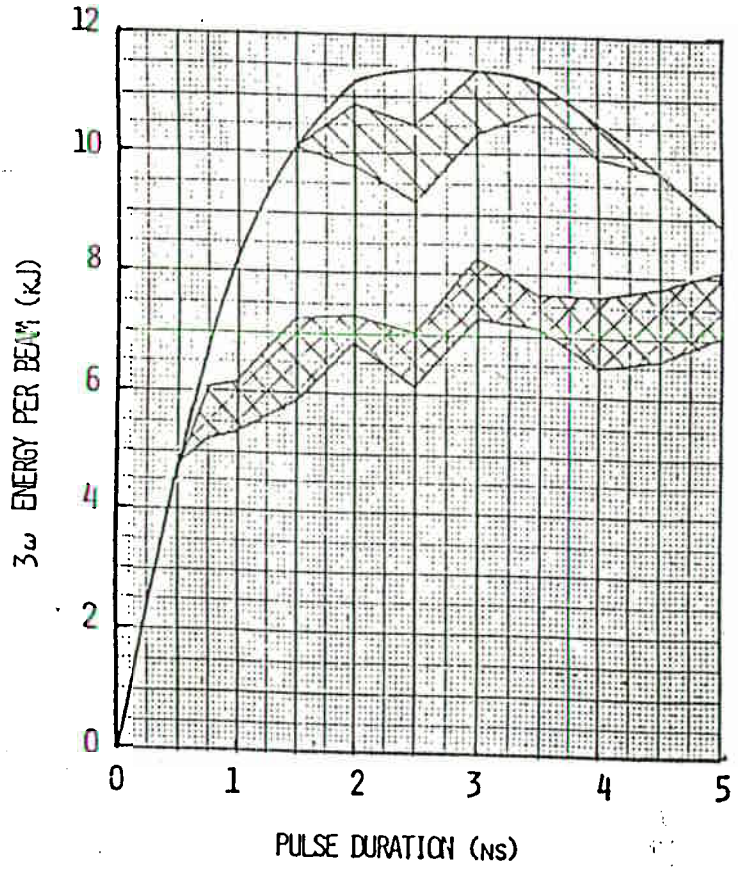

15-cm KDP

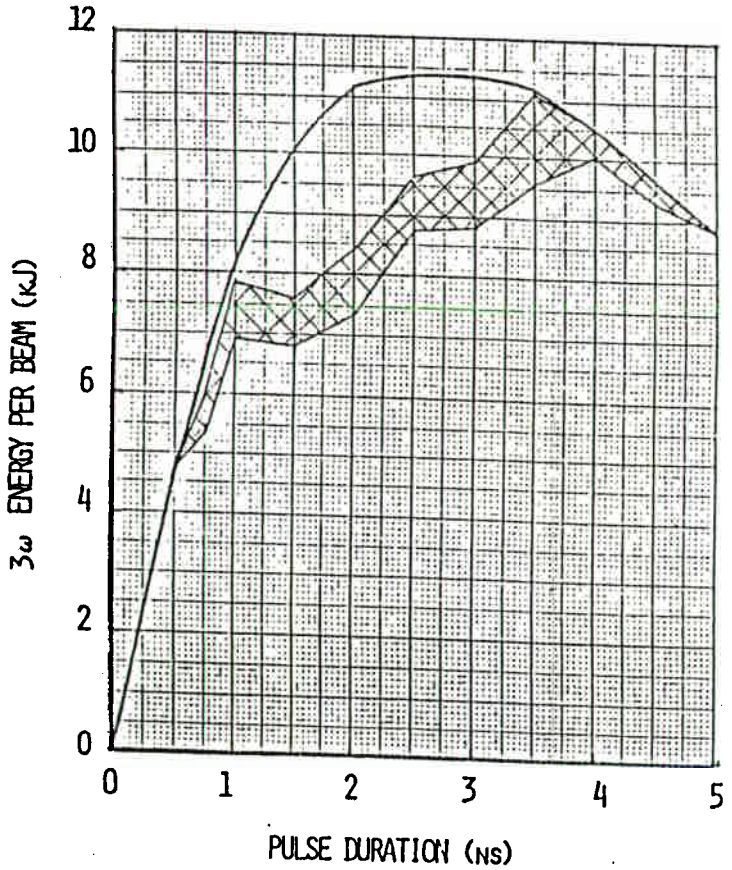

POTENTIAL REDUCTION IN 2ω OUTPUT OF A NON-PARTITIONED, 74 CM KDP ARRAY

DUE TO QUASI-CONSTANT OUTPUT FLUENCE OF NOVA/NOVETTE, SRS LOSS PROBLEM IN KDP ARRAYS IS ALMOST APERTURE-INDEPENDENT

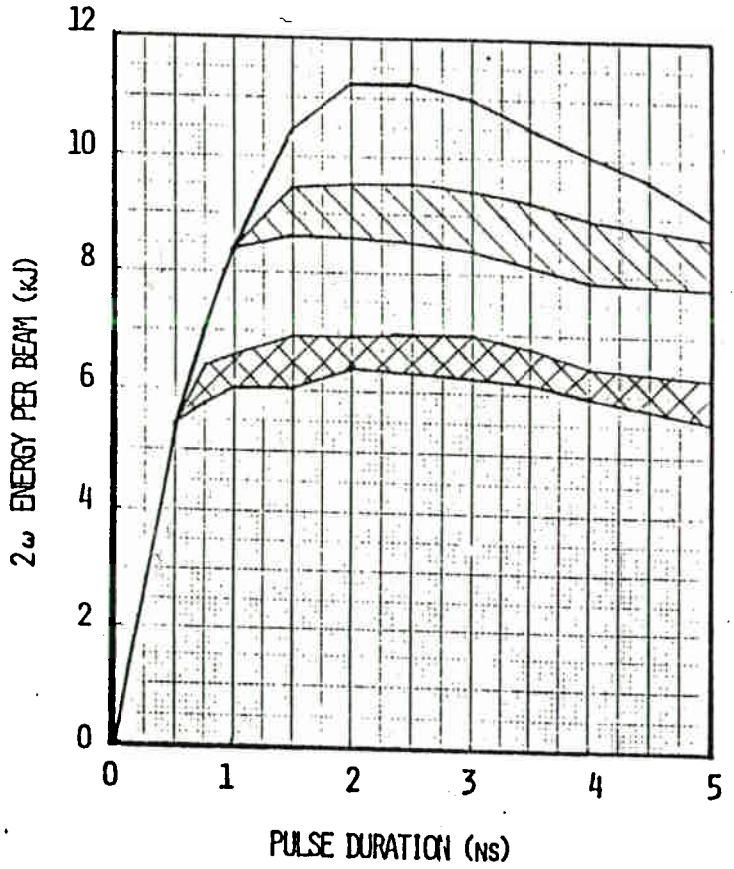

FIG. 16

Distribution

Ahlstrom, H. G.	L-481
Attwood, D. T.	L-479
Bliss, E. S.	L-492
Bradley, L. P.	L-470
Campbell, E. M.	L-473
Carder, B. M.	L-470
Coleman, L. W.	L-473
Eimerl, D.	L-470
Emmett, J. L.	L-488
Falk, J.	L-472
George, E. V.	L-481
Godwin, R. O.	L-493
Goldhar, J.	L-470
Haas, R. A.	L-472
Hagen, W. F.	L-470
Haussmann, A. C.	L-28
Hendricks, C. D.	L-482
Henesian, M. A.	L-472
Hopper, R.	L-470
Holzrichter, J. F.	L-481
Hunt, J. T.	L-470
Hurley, C. A.	L-495
Johnson, B. C.	L-495
Krupke, W. F.	L-488
Kuizenga, D. J.	L-495
Lowdermilk, W. H.	L-470
Manes, K. R.	L-493
Marchi, F. T.	L-491
Milam, D.	L-470
Monsler, M. J.	L-481
Murray, J. E.	L-470
Murray, J. R.	L-470
Nuckolls, J. H.	L-477
Ozarski, R. G.	L-492
Pleasance, L. D.	L-470
Powell, H. T.	L-470
Rainer, F.	L-470
Rescigno, R. N.	L-472
Rienecker, F.	L-495
Schlitt, L. G.	L-470
Seppala, L. G.	L-491
Simmons, W. W.	L-493
Sooy, W.	L-488
Speck, D. R.	L-493
Stokowski, S. E.	L-491
Stowers, I. F.	L-482
Summers, M. A.	L-493
Suski, G. J.	L-493
Swain, J. E.	L-470
Trenholme, J. B.	L-472
Wallerstein, E. P.	L-491
Warren, W. E.	L-471
Weber, M. J.	L-472
White, T.	L-471